Nonrelativistic structure calculations of two-electron ions in a strongly coupled plasma environment

S. Bhattacharyya,[1,*] J. K. Saha,[2] and T. K. Mukherjee[3]
[1]*Acharya Prafulla Chandra College, New Barrackpore, Kolkata 700131, India*
[2]*Indian Association for the Cultivation of Science, Jadavpur, Kolkata 700032, India*
[3]*Narula Institute of Technology, Agarpara, Kolkata 700109, India*
(Received 19 March 2015; published 30 April 2015)

In this work, the controversy between the interpretations of recent measurements on dense aluminum plasma created with the Linac coherent light source (LCLS) x-ray free electron laser (FEL) and the Orion laser has been addressed. In both kinds of experiments, heliumlike and hydrogenlike spectral lines are used for plasma diagnostics. However, there exist no precise theoretical calculations for He-like ions within a dense plasma environment. The strong need for an accurate theoretical estimate for spectral properties of He-like ions in a strongly coupled plasma environment leads us to perform *ab initio* calculations in the framework of the Rayleigh-Ritz variation principle in Hylleraas coordinates where an ion-sphere potential is used. An approach to resolve the long-drawn problem of numerical instability for evaluating two-electron integrals with an extended basis inside a finite domain is presented here. The present values of electron densities corresponding to the disappearance of different spectral lines obtained within the framework of an ion-sphere potential show excellent agreement with Orion laser experiments in Al plasma and with recent theories. Moreover, this method is extended to predict the critical plasma densities at which the spectral lines of H-like and He-like carbon and argon ions disappear. *Incidental degeneracy* and *level-crossing* phenomena are being reported for two-electron ions embedded in strongly coupled plasma. Thermodynamic pressure experienced by the ions in their respective ground states inside the ion spheres is also reported.

DOI: 10.1103/PhysRevA.91.042515 PACS number(s): 31.15.ac, 31.15.vj, 52.27.Gr, 32.10.Hq

I. INTRODUCTION

The study of confined quantum mechanical systems has attracted immense attention from researchers around the world due to the novel and unusual structural properties exhibited by such systems when subject to spatial limitation [1]. A wide variety of physical situations are manifested in nature that relates to spatially confined systems such as atoms or molecules trapped in zeolite sieves [2], fullerenes [3], plasma environment [4], solvent environment [5], under high pressure in the walls of nuclear reactors [6], quantum dot or artificial atom [7], molecular containers, storage of fuel cells [8,9], matter under high pressure in Jovian planets [10], etc. Along with the experimental and technological development, theoretical research plays a fundamental role in designating appropriate models in order to explore and predict the behavioral changes of a confined system. The present study is focused on atomic systems embedded in a plasma environment. In recent years, atoms placed in an external plasma environment have received considerable attention from researchers [11–19] due to their wide applications in various disciplines of science, e.g., astrophysics, condensed matter physics, biology, etc. While dealing with plasma that follows classical statistics, a coupling parameter (Γ) defined as the ratio of the average electrostatic energy and the average thermal energy is introduced. $\Gamma < 1$ corresponds to weakly coupled plasma (WCP) for which the effective potential experienced by the embedded ion is expressed according to the *Debye* model [20] and $\Gamma \geqslant 1$ denotes strongly coupled plasma (SCP) where the potential is taken (present case) from the ion-sphere (IS) model [21]. It should be mentioned that there are other models also for dealing with plasma environments such as the "muffin-tin" model [22], "fried egg" model [23], neutral-pseudoatom (NPA) model [24], etc. According to the average-atom IS model, a sphere (termed as the *Wigner-Seitz sphere*) surrounding a positively charged ion is considered in such a way that the plasma electrons within the sphere neutralize the positive ion. The size of the *Wigner-Seitz* sphere will decrease when the number density of plasma electrons (n_e) increases. The temperature (T) of the plasma does not appear directly in this model but it is implicit as n_e is different for different temperatures for a given Γ. The domain of the effective potential representing the SCP surrounding is finite in the case of the IS model in contrast to the long-range character of the screened Coulomb potential used in the *Debye* model [20] for the WCP environment. The examples of WCP's are the gaseous discharge plasma ($T \sim 10^4$ K and $n_e \sim 10^{11}/\text{cm}^3$), plasma in controlled thermonuclear reaction ($T \sim 10^8$ K and $n_e \sim 10^{16}/\text{cm}^3$), solar coronal plasma ($T \sim 10^6$–10^8 K and $n_e \sim 10^6$–$10^{10}/\text{cm}^3$), Tokamak plasma ($T \sim 10^5$–10^7 K and $n_e \sim 10^8$–$10^{16}/\text{cm}^3$), etc. SCP's (temperature varies and typical densities $\geqslant 10^{23}/\text{cm}^3$) are observed in highly evolved stars in high density states, the interior of Jovian planets, explosive shock tubes, two-dimensional states of electrons trapped in surface states of liquid helium, laser-produced plasmas, etc. Spectral line shifts, pressure ionization, ionization potential depression (IPD), and line merging phenomena occur in the plasma environment, both strongly and weakly coupled, due to the deformation of the ionic potential by the plasma fields which may be viewed in several ways [20,21,25,26]. It is now well established [27–30] that the dynamic shifts can be as large as static ones. At the same time, for highly polarizable states [31], a weak collision can ionize the system or can produce resonance states. Such properties and knowledge about ion-plasma interaction can effectively be utilized for

*sukhamoy.b@gmail.com

diagnostics and the investigation of x-ray opacity of matter under conditions prevailing in stellar interiors. In the present work, we concentrate upon SCP only since the temperature is low so that we can neglect dynamics, e.g., collisions. The experimental observations using laser-produced plasmas for C, Al, and Ar by Nantel *et al.* [32], Saemann *et al.* [33], and Woolsey *et al.* [34] have explicitly demonstrated the effect of SCP on the spectral properties of such systems. The laboratory plasma conditions (T and n_e) undergo rapid changes with respect to where local thermodynamic equilibrium is not maintained. Consequently, the experimental measurements become extremely complicated leading to a loss of accuracy and, until the end of the last century, this accuracy level was not even mentioned in most of the experiments.

In recent years, a remarkable improvement has been made [35–38] with the advent of Linac coherent light sources (LCLS) towards the creation of relatively long-lived high-density plasma at homogeneous temperature and densities. In these experiments, an x-ray free-electron laser (FEL) was used to create plasma with densities up to almost one order higher than solid Al and then spectral line profiles of different charge states of Al were used for diagnostics. The effect of IPD on the emitted spectra as a function of n_e is explored experimentally by observing the disappearance of spectral lines of H-like and He-like Al. During the observation of K-shell fluorescence of highly charged Al, Ciricosta *et al.* [37] found that the IPDs measured were not consistent with the predictions of the most widely used theoretical model of Stewart and Pyatt (SP) [39] but in good agreement with an earlier model due to Ecker and Kröll (EK) [40]. However, this observation was questioned in a subsequent theoretical study by Preston *et al.* [41] where detailed simulations were carried out for the spectral lines of H-like and He-like Al to study IPD by using both SP and EK (in a modified form) models. In experiments, the intensities and Stark-broadened widths of He-β and Ly-β spectral lines are used for main diagnostics. A direct measurement of ionization potential depression is a difficult task because of its indistinguishability from the effect of spectral line merging due to Stark broadening [42]. Hoarty *et al.* [43,44] have been able to overcome this difficulty and their measurements for Al plasma using the Orion laser are in closer agreement with the SP model of IPD than the EK model. This situation clearly warrants extensive and accurate *ab initio* study of atomic structures; within the dense plasma environment a few theoretical approaches are made so far [45–47]. Son *et al.* [47] have adopted a two-step Hartree-Fock-Slater approach to assess the IPD effect for Al^{3+} to Al^{7+} within plasma where a muffin-tin flat potential was used. The IPDs calculated by Son *et al.* [47] lie between the SP and modified EK models and in some cases, are close to the SP model. But so far, no extensive theoretical calculation on IPDs for He-like ions has been performed. It should be noted here that both the SP model and the EK model for estimating IPDs are derived within the framework of the IS potential. The only theoretical work for He-like ions in the field of SCP by using the IS potential is due to Sil *et al.* [48] where both nonrelativistic and relativistic calculations were carried out using time-dependent perturbation theory. They have included the IS potential in the unperturbed Hamiltonian and then applied a harmonic perturbation to probe the dipole transitions to low-lying excited states from the ground state. Although Sil *et al.* [48] demonstrated that the relativistic IS model yields consistent results in predicting the spectral line positions for the systems considered, some anomalies such as better agreement of nonrelativistic results with experiments than relativistic ones are observed in their data [48]. Such strange features may arise due to improper inclusion of electron correlation in the basis set within a finite region. A major challenge for precise theoretical calculations is, therefore, to develop an appropriate methodology where the effect of electron correlations within a finite domain is aptly included.

To the best of our knowledge, there exists no calculation of He-like atoms embedded in SCP using the Hylleraas-type basis set although it is well accepted that within the framework of the Ritz variational technique, explicitly correlated wave functions expanded in terms of the Hylleraas basis (and its variants) can produce most accurate nonrelativistic energies of He-like atoms. These methods have been applied extensively to free He-like systems whereas for spatially confined two-electron systems, such studies are limited to S states only [49–52]. According to Laughlin and Chu [51], the generalized Hylleraas basis sets used in such calculations suffer the loss of linear independence for large dimensions of the wave functions and hence all the calculations [49–52] were limited to small dimensions (at best 25). Laughlin and Chu [51] made an effort to remove this difficulty and extended the basis size up to 95 parameters where they have to compromise with the flexibility of the nonlinear parameters. Recently, for $^1S^e$ states of He-like systems under spherical confinement, the present authors have calculated the energy values [53] by using the standard Hylleraas basis set of dimension 161 and the results have been confirmed by Montgomery and Pupyshev [54]. In the present work, a successful effort has been made to develop a general methodology in the Hylleraas basis for both the S and P states of He-like systems. The finite domain two-electron integrals with flexible parameters are evaluated where the problem of linear dependency in larger dimensions is clearly avoided.

We have estimated precise nonrelativistic energy values of $1sns$ ($^1S^e$) [n =1–3] and $1sn'p$ ($^1P^o$) [n' =2–4] states of He-like C, Al, and Ar within the SCP environment. Accuracy of the computed energy eigenvalues have been tested systematically over an extended range of parameters and also by increasing the number of terms (N) in the expanded basis sets. The plasma densities (n_e) are varied from a low value that corresponds to almost a free system to a very high one that leads the ion towards destabilization (i.e., the energy becomes zero). The plasma electron densities in different experimental conditions [32–38,43] are well covered within the density ranges studied here. The energy eigenvalues of ns (^2S) [n = 1–2] and $n'p$ (^2P) [n' = 2–3] states of H-like C, Al, and Ar in SCP are also estimated to determine the variation of ionization potential (IP) with respect to n_e. As n_e increases, both the two-electron excited states as well as the respective one-electron threshold move towards destabilization, thereby reducing the IP. It is remarkable that after a certain value of n_e, the two-electron energy levels move above the respective one-electron energy level and become quasibound. *Incidental degeneracy* [55] and subsequent *level-crossing* phenomenon between the excited

states such as $1s2s$ ($^1S^e$) and $1s2p$ ($^1P^o$) under SCP have been observed. Due to spatial restriction imposed upon the wave function according to the IS model under the SCP environment, the ion will feel a pressure inside the *Wigner-Seitz* sphere. The variation of thermodynamic pressure with respect to plasma density is also calculated. The paper is organized as follows: An outline of the basic theory used and details on the evaluation of the basis integrals are given in Sec. II, followed by a discussion of the results in Sec. III, and finally concluding in Sec. IV with a view towards further application of the present methodology in related fields.

II. METHOD

The nonrelativistic Hamiltonian (in a.u.) of a two-electron ion placed inside the SCP environment can be written as

$$H = \sum_{i=1}^{2}\left[-\frac{1}{2}\nabla_i^2 + V_{\rm IS}(r_i)\right] + \frac{1}{r_{12}}. \tag{1}$$

$V_{\rm IS}(r_i)$ is the one-electron term of the modified potential energy as "*seen*" by the ith electron within the ion sphere. It is to be noted that in this model, the electronic repulsion part in the potential is completely unaltered. The spherically symmetric potential $V_{\rm IS}(r_i)$ experienced by a positive charge ion surrounded by a one-component plasma within the ion sphere [21] is given by

$$V_{\rm IS}(r_i) = -\frac{Z}{r_i} + \frac{(Z-N_e)}{2R}\left[3 - \left(\frac{r_i}{R}\right)^2\right]. \tag{2}$$

The radius of the ion-sphere R is known as the *Wigner-Seitz* radius [21]. Z is the nuclear charge and N_e ($<Z$) is the number of bound electrons present in the ion. $N_e = 1$ and 2 for H-like and He-like ions. The Schrodinger equation $H\Psi = E\Psi$ is to be solved to obtain the energy eigenvalues where the wave function is subject to the normalization condition $\langle\Psi|\Psi\rangle = 1$ within the sphere. The structure of the potential demands that no electron current is taking place through the boundary surface of the *Wigner-Seitz* sphere, and the orbital wave function Ψ satisfies the boundary condition,

$$\Psi(r) = 0, \quad \text{at} \quad r \geqslant R. \tag{3}$$

This boundary condition plays a significant role in behavioral changes of the confined atoms. The plasma electrons within the ion-sphere neutralize the central positive charge and the size of the *Wigner-Seitz* sphere is determined by the condition of overall charge neutrality that yields

$$R = \left[\frac{3(Z-N_e)}{4\pi n_e}\right]^{\frac{1}{3}}. \tag{4}$$

The above expression for "R" is used to determine the IPD according to the SP model [39]. However, in the EK model [40] for determining the IPD, this radius was calculated in a somewhat different way where both the electron density (n_e) and ion density (n_i) are considered. According to the EK model [40], the radius of the sphere would be expressed as

$$R_{\rm EK} = \left[\frac{3}{4\pi(n_e+n_i)}\right]^{\frac{1}{3}}. \tag{5}$$

From now on, R will always refer to the IS radius unless mentioned otherwise.

Due to the translational symmetry of the Hamiltonian, the degrees of freedom of a two-electron ion reduce from nine to six by separating the motion of the center of mass. These six coordinates can be taken as the sides of the triangle r_1, r_2, r_{12} formed by the three particles, i.e., two electrons and the fixed nucleus and the Eulerian angles (θ,ϕ,ψ) defining the orientation of this triangle in space. The wave function obeying symmetry properties under the particle exchange may be written as [56]

$$\Psi\left(\vec{r_1},\vec{r_2}\right) = \sum_{\kappa}\left[f_L^{\kappa+}(r_1,r_2,\theta_{12})\,D_L^{\kappa+}(\theta,\phi,\psi) + f_L^{\kappa-}(r_1,r_2,\theta_{12})\,D_L^{\kappa-}(\theta,\phi,\psi)\right]. \tag{6}$$

θ_{12} is the angle between $\vec{r_1}$ and $\vec{r_2}$. The summation in Eq. (6) goes over every alternate value of κ, where $\kappa = |k|$. k is the angular momentum quantum number about the body fixed axis of rotation whose value satisfies $k \leqslant L$, L being the total angular momentum quantum number. The symmetric top functions $D_L^{\kappa+}$ and $D_L^{\kappa-}$ are the eigenfunctions of the angular momentum operator L^2 of the two electrons. The rotational invariance of the Hamiltonian makes it possible to express the variational equation of two electrons in the field of a fixed nucleus in terms of three independent variables r_1, r_2, and r_{12} (or θ_{12}). The reduction of the Eulerian angles from the variational equation is an immediate consequence of the spherical symmetry of the field. The variational equations (derived from the general equation given in Ref. [57]) for $1sns$ ($^1S^e$) states and $1snp$ ($^1P^o$) are taken from Ref. [53] and Ref. [58], respectively. The correlated functions are of the form,

$$f(r_1,r_2,r_{12}) = (R-r_1)(R-r_2)g(r_1,r_2,r_{12}), \tag{7}$$

where

$$g(r_1,r_2,r_{12}) = e^{-\sigma_1 r_1-\sigma_2 r_2}\sum_l\sum_m\sum_n C_{lmn}r_1^l r_2^m r_{12}^n. \tag{8}$$

This correlated function ensures that the wave function vanishes at the boundary of the *Wigner-Seitz* sphere. This is due to the fact that, according to the IS model, the local thermodynamic equilibrium is maintained within the *Wigner-Seitz* sphere where the charge neutrality condition is locally satisfied. The effect of the radial correlation is introduced in the wave function through the nonlinear parameters σ_1 and σ_2 whereas the angular correlation effect is incorporated through different powers of r_{12}. C's are the linear variational parameters. The total number of parameters (N) in the basis set is defined as the total number of different (l,m,n) sets [Eq. (8)] taken in the expansion of $f(r_1,r_2,r_{12})$. The optimized values of nonlinear parameters in Eq. (7) are obtained by using the Nelder-Mead algorithm [59]. The linear variational parameters along with the energy eigenvalues are obtained by solving the generalized eigenvalue equation,

$$\underline{\underline{H}}\,\underline{C} = E\,\underline{\underline{S}}\,\underline{C}, \tag{9}$$

where $\underline{\underline{H}}$ is the Hamiltonian matrix, $\underline{\underline{S}}$ is the overlap matrix, $\underline{C}$ is the column matrix consisting of linear variational parameters, and E is the corresponding energy eigenvalue. The wave function is normalized for each confining radius R

to account for the reorientation of charge distribution within the *Wigner-Seitz* sphere. All computations are carried out in quadruple precision.

The radial function $\chi(r)$ for one-electron ions is given by

$$\chi(r) = (R-r)r^k \sum_i C_i e^{-\rho_i r}, \tag{10}$$

where $k = 0$ and 1 for the ^2S and ^2P states, respectively. In this calculation, we have taken 21 different nonlinear parameters (ρ_i's) in a geometrical sequence $\rho_i = \rho_{i-1}\gamma$, γ being the geometrical ratio [13,60]. Such choice of nonlinear parameters enables us to cover the full region of space in a flexible manner by adjusting γ. The energy values and linear coefficients are determined by using Eq. (9).

The pressure experienced by an ion embedded in plasma may be realized from the IS model that demands a truncation of the wave function at a finite distance [Eq. (3)]. We have calculated the pressure felt by all the H-like and He-like ions in their respective ground states using the first law of thermodynamics. However, for excited states having a finite lifetime, this approach is not valid as the equilibrium criteria is not maintained. Under an adiabatic approximation, the pressure on the ions in the ground state can be expressed as [53]

$$P = -\frac{1}{4\pi R^2}\frac{dE}{dR}. \tag{11}$$

Evaluation of two-electron integrals

The correlated two-electron basis integrals arising in the present calculations are of the form,

$$\begin{aligned} &A(a,b,c;\alpha,\beta;R) \\ &= \int_0^R r_1^a e^{-\alpha r_1} \int_0^R r_2^b e^{-\beta r_2} \int_{|r_1-r_2|}^{r_1+r_2} r_{12}^c dr_1 dr_2 dr_{12} \\ &= \int_0^R r_1^a e^{-\alpha r_1} \int_0^{r_1} r_2^b e^{-\beta r_2} \int_{r_1-r_2}^{r_1+r_2} r_{12}^c dr_1 dr_2 dr_{12} \\ &\quad + \int_0^R r_2^b e^{-\beta r_2} \int_0^{r_2} r_1^a e^{-\alpha r_1} \int_{r_2-r_1}^{r_1+r_2} r_{12}^c dr_1 dr_2 dr_{12}. \end{aligned} \tag{12}$$

For S states, $a \geqslant 0, b \geqslant 0, c \geqslant 0$ while for higher angular momentum states (P, D, etc.), integrals with $a = -1$ also arise. After integration, the r_{12} part of Eq. (12) can be expanded as

$$\begin{aligned} &\frac{1}{n+1}[(r_1+r_2)^{n+1} - (r_1-r_2)^{n+1}] \\ &= \sum_{i=0}^{\frac{n}{2}} \frac{2.n!}{(2i+1)!(n-2i)!} r_1^{n-2i} r_2^{2i+1} \quad [n \text{ even}]. \end{aligned} \tag{13}$$

For odd 'n', the upper limit of the sum in the right-hand side would be replaced by $\frac{n-1}{2}$. The integrals from Eq. (12) then reduce to the form,

$$\begin{aligned} \int_0^y x^k e^{-\lambda x} dx &= \int_0^\infty x^k e^{-\lambda x} dx - \int_y^\infty x^k e^{-\lambda x} dx \\ &= \frac{k!}{\lambda^{k+1}} \left[1 - e^{-\lambda y} \sum_{j=0}^{k} \frac{y^j \lambda^j}{j!} \right]. \end{aligned} \tag{14}$$

λ is a positive real number and k is a non-negative integer and we have used the standard integral,

$$\int_0^\infty x^k e^{-\lambda x} dx = \frac{k!}{\lambda^{k+1}}. \tag{15}$$

The integral $A(a,b,c;\alpha,\beta;R)$ is now evaluated for two different cases.

Case I: $a \geqslant 0, b \geqslant 0, c \geqslant 0$

An exact analytical expression for $A(a,b,c;\alpha,\beta;R)$ corresponding to $a \geqslant 0, b \geqslant 0, c \geqslant 0$ has been derived in a straightforward way using Eq. (14) and the numerical values are displayed in Table I. In the first column of Table I, different powers of r_1, r_2, and r_{12}, i.e., a, b, and c are given. For each set of (a,b,c), the nonlinear parameters (α,β) given in the second column of Table I are varied from very low to high values as obtained from the optimized values corresponding to different cases in the present work. R varies in a wide range for each set of (a,b,c,α,β). The values of integrals are given in the last column of Table I. The results match exactly with those obtained from standard mathematical software (e.g., MAPLE), which ensure the numerical accuracy of the expression for $A(a,b,c;\alpha,\beta;R)$ over the complete range of R.

Case II: $a = -1, b \geqslant 0, c \geqslant 0$

After full expansion of the integral $A(-1,b,c;\alpha,\beta;R)$ over r_{12} and r_2 by using Eqs. (13) and (14), an integral $I(\alpha,\beta;R)$ arises which takes the form,

$$I(\alpha,\beta;R) = \int_0^R \frac{e^{-\alpha r_1} - e^{-(\alpha+\beta)r_1}}{r_1} dr_1. \tag{16}$$

The above integral $I(\alpha,\beta;R)$ is actually a converging infinite series with oscillatory terms. We have tested the evaluation of the term $I(\alpha,\beta;R)$ in two different approaches.

(i) We can expand the exponential functions to evaluate the integral as

$$\begin{aligned} &\int_0^R \frac{e^{-\alpha r_1} - e^{-(\alpha+\beta)r_1}}{r_1} dr_1 \\ &= \sum_{q=0}^{\infty} \int_0^R \frac{1}{r_1} \left[\frac{(-1)^q}{q!} \{\alpha^q - (\alpha+\beta)^q\} r_1^q \right] dr_1 \\ &= \sum_{q=1}^{\infty} \frac{(-1)^q R^q}{q\,q!} [\alpha^q - (\alpha+\beta)^q]. \end{aligned} \tag{17}$$

The expression (17) gives an accurate value of integrals where the upper limit R is small, but fails to produce results when R is sufficiently high.

(ii) Alternatively, the integral $I(\alpha,\beta;R)$ may be written as

$$\begin{aligned} &\int_0^R \frac{e^{-\alpha r_1} - e^{-(\alpha+\beta)r_1}}{r_1} dr_1 \\ &= \int_0^R \frac{e^{-\alpha r_1}}{r_1} (1 - e^{-\beta r_1}) dr_1 \\ &= \sum_{q=1}^{\infty} \frac{(-1)^{q-1}\beta^q}{q!} \int_0^R r_1^{q-1} e^{-\alpha r_1} dr_1. \end{aligned} \tag{18}$$

TABLE I. Values of integral $A(a,b,c;\alpha,\beta;R)$ with $a \geqslant 0, b \geqslant 0, c \geqslant 0$. The notation $x[y]$ indicates $x \times 10^y$.

(a,b,c)	α	β	R	$A(a,b,c;\alpha,\beta;R)$
(0,0,0)	0.62 450 527	0.41 287 135	100.0	0.7 477 263 489 878 847 [+01]
			2.0	0.1 578 745 363 918 980 [+01]
			0.2	0.4 688 300 923 274 260 [−02]
	8.92 934 001	5.97 270 373	100.0	0.2 516 482 004 376 827 [−02]
			2.0	0.2 516 454 642 411 431 [−02]
			0.2	0.9 770 367 665 657 275 [−03]
	17.42 010 556	10.32 300 145	100.0	0.4 008 834 505 965 748 [−03]
			2.0	0.4 008 834 499 068 468 [−03]
			0.2	0.3 006 046 149 224 955 [−03]
(2,3,1)	0.62 450 527	0.41 287 135	100.0	0.1 578 244 631 585 587 [+06]
			2.0	0.9 755 441 256 974 906 [+01]
			0.2	0.4 326 241 505 739 082 [−07]
	8.92 934 001	5.97 270 373	100.0	0.5 960 191 090 886 659 [−05]
			2.0	0.5 913 015 230 723 085 [−05]
			0.2	0.4 824 781 046 773 954 [−08]
	17.42 010 556	10.32 300 145	100.0	0.2 667 837 768 848 479 [−07]
			2.0	0.2 667 811 045 194 153 [−07]
			0.2	0.7 198 650 559 020 197 [−09]
(3,4,6)	0.62 450 527	0.41 287 135	100.0	0.5 959 047 433 004 562 [+14]
			2.0	0.3 133 286 105 045 369 [+04]
			0.2	0.1 612 293 542 969 925 [−11]
	8.92 934 001	5.97 270 373	100.0	0.1 741 465 133 115 703 [−04]
			2.0	0.1 311 556 348 743 337 [−04]
			0.2	0.1 427 263 707 660 009 [−12]
	17.42 010 556	10.32 300 145	100.0	0.1 312 396 696 573 856 [−08]
			2.0	0.1 305 938 614 015 103 [−08]
			0.2	0.1 601 541 647 520 373 [−13]

The r_1 integral in the right-hand side of Eq. (18) is then evaluated using Eq. (14).

The integral $I(\alpha,\beta;R)$ is calculated by using both the expressions given in Eqs. (17) and (18). All the results corresponding to different sets of $(\alpha,\beta;R)$ are given in Table II which shows excellent agreement among the results except for some high values of R used in Eq. (17). On the other hand, Eq. (18) yields excellent results over the complete range of R. In Eq. (17), a term R^q appears in the numerator that increases with increase in q. For low values of R, this term is

TABLE II. Values of integral $I(\alpha,\beta;R)$. Results obtained by using Eqs. (17) and (18) are given in consecutive rows, respectively. The notation $x[y]$ indicates $x \times 10^y$.

α	β	R	$I(\alpha,\beta;R)$
0.62 450 527	0.41 287 135	100.0	0.2 910 109 651 677 626 [+9]
			0.5 074 905 562 702 974
		2.0	0.4 049 645 534 617 721
			0.4 049 645 534 617 721
		0.2	0.0 760 845 585 264 357
			0.0 760 845 585 264 357
8.92 934 001	5.97 270 373	100.0	0.2 617 916 518 793 351 [+602]
			0.5 121 558 822 014 390
		2.0	0.5 121 558 812 688 812
			0.5 121 558 812 688 812
		0.2	0.4 595 083 872 393 843
			0.4 595 083 872 393 843
17.42 010 556	10.32 300 145	100.0	0.9 419 309 325 371 151 [+872]
			0.4 653 623 821 935 131
		2.0	0.4 653 623 821 935 052
			0.4 653 623 821 935 131
		0.2	0.4 588 587 688 120 597
			0.4 588 587 688 120 597

TABLE III. Convergence of the integral $I(\alpha,\beta;R)$ with respect to the number of terms (q) in the infinite series using Eqs. (17) and (18). The notation $x[y]$ indicates $x \times 10^y$.

				$I(\alpha,\beta;R)$	
α	β	R	q	Eq. (17)	Eq. (18)
0.62 450 527	0.41 287 135	100	10	−0.3 568 526 587 566 828 [+13]	0.5 068 930 031 430 272
			20	−0.3 554 037 122 215 343 [+21]	0.5 074 856 438 054 664
			50	−0.2 755 048 215 770 421 [+35]	0.5 074 905 562 626 217
			100	−0.2 124 755 543 448 736 [+42]	0.5 074 905 562 702 974
			1000	0.2 910 109 651 677 626 [+09]	0.5 074 905 562 702 974
		0.2	10	0.0 760 845 585 264 356	0.0 760 845 585 264 357
			20	0.0 760 845 585 264 357	0.0 760 845 585 264 357
			50	0.0 760 845 585 264 357	0.0 760 845 585 264 357
			100	0.0 760 845 585 264 357	0.0 760 845 585 264 357
			1000	0.0 760 845 585 264 357	0.0 760 845 585 264 357
17.42 010 556	10.32 300 145	100	10	−0.7 343 514 275 041 944 [+27]	0.4 651 757 934 474 452
			20	−0.1 488 071 327 579 564 [+50]	0.4 653 618 680 730 945
			50	−0.9 285 235 939 919 110 [+106]	0.4 653 623 821 934 812
			100	−0.2 137 812 095 536 411 [+185]	0.4 653 623 821 935 131
			1000	−0.2 609 904 279 835 017 [+873]	0.4 653 623 821 935 131
		0.2	10	0.2 166 573 622 291 603	0.4 588 585 238 460 869
			20	0.4 588 555 852 277 264	0.4 588 587 688 120 596
			50	0.4 588 587 688 120 597	0.4 588 587 688 120 597
			100	0.4 588 587 688 120 597	0.4 588 587 688 120 597
			1000	0.4 588 587 688 120 597	0.4 588 587 688 120 597

balanced by $q!$ in the denominator but for high R, a numerical instability appears because within the first few terms, R^q bounces more rapidly than $q!$. In contrast, a term $\frac{R^j}{j!}e^{-\alpha R}$ appears in Eq. (18) [after expanding the r_1 integral according to Eq. (14)] which falls rapidly as q increases due to the presence of the exponential term. To have a better understanding of the integrals, we have also checked the convergence of $I(\alpha,\beta;R)$ evaluated using Eqs. (17) and (18) by increasing the number of terms in the infinite series and displayed the convergence behavior in Table III for $R = 100.0$ and 0.2 a.u. and two sets of (α,β). It appears from Table III that for $R = 100.0$ a.u. the values derived from Eq. (17) are clearly not acceptable but for low R, the final results match exactly although the convergence is slow for Eq. (17). We have finally used Eq. (18) to calculate the energy eigenvalues in the present work and taken 1000 terms in the corresponding infinite series to ensure the desired level of accuracy. In Table IV we have given the values of integral $A(-1,b,c;\alpha,\beta;R)$ corresponding to different sets of parameters. We have further observed that the integrals [Eq. (18)] corresponding to $R = 100$ a.u. yield the same result as obtained by using Eq. (15) for $R = \infty$. This is to mention further that all the integrals are checked with standard mathematical software.

III. RESULTS AND DISCUSSIONS

The energy eigenvalues of He-like C, Al, and Ar in $1sns(\,^1S^e)$ [n =1–3] and $1sn'p(\,^1P^o)$ [n' =2–4] states have been calculated within the SCP environment using the IS potential. We have studied the convergence of the energy values with respect to the number of terms (N) in the wave function. Table V shows the convergence behavior of C^{4+} in the $1s^2(\,^1S^e)$ state for some selected values of R. We have obtained a similar convergence pattern for all the other ions and also for the excited states under consideration. The size of the basis has been extended systematically to $N = 161$ and 149 for the $^1S^e$ and $^1P^o$ states, respectively, with $l + m + n = 10$ [Eq. (8)]. The convergence of the energy values are obtained at least up to the sixth significant digits. In fact, for some cases, e.g., the $1s^2(\,^1S^e)$ state of C^{4+} with $R = 0.47$ a.u., we have obtained convergence of energy values up to the eighth decimal place, as is evident from Table V. The above observation ensures that the present method can deal with extended basis sets to yield sufficiently accurate energy values within a finite limit.

The energy values of He-like C, Al, and Ar in $1sns(\,^1S^e)$ [n = 1–3] and $1sn'p(\,^1P^o)$[n' = 2–4] states within the ion sphere of different radii (R) are displayed in Tables VI–VIII, respectively. We have also listed the energies of respective H-like ions in ns (^2S) [n = 1–2] and $n'p$ (^2P) [n' = 2–3] states. It is worthwhile to mention that under one-component plasma approximation, the IS radius for a two-electron ion would differ from that for a one-electron ion corresponding to the same plasma electron density. We see that as n_e increases, the energy levels move towards continuum which is a clear manifestation of the positive nature of the IS potential. To check the overall behavior of the results, we have plotted the energy values ($-E$) of bound $1sns$ ($^1S^e$) [n = 1–3] and $1sn'p$ ($^1P^o$) [n' = 2–4] states of C^{4+} with respect to the IS radius (R) in Figs. 1(a) and 1(c), respectively. It is evident from Figs. 1(a) and 1(c) that the energy values remain almost unaltered for large enough R while for small

TABLE IV. Values of integral $A(a,b,c;\alpha,\beta;R)$ with $a=-1, b\geqslant 0, c\geqslant 0$. The notation $x[y]$ indicates $x\times 10^{y}$.

(a,b,c)	α	β	R	$A(-1,b,c;\alpha,\beta;R)$
(−1,0,0)	0.62 450 527	0.41 287 135	100.0	0.5 954 269 203 657 702 [+01]
			2.0	0.2 328 753 595 641 012 [+01]
			0.2	0.5 410 340 957 954 025 [−01]
	8.92 934 001	5.97 270 373	100.0	0.2 871 376 988 672 015 [−01]
			2.0	0.2 871 352 649 435 828 [−01]
			0.2	0.1 630 927 123 879 263 [−01]
	17.42 010 556	10.32 300 145	100.0	0.8 733 921 675 818 471 [−02]
			2.0	0.8 733 921 663 803 946 [−02]
			0.2	0.7 244 151 319 038 541 [−02]
(−1,3,0)	0.62 450 527	0.41 287 135	100.0	0.6 567 231 700 864 201 [+03]
			2.0	0.4 615 410 090 669 881 [+01]
			0.2	0.1 352 981 404 883 989 [−03]
	8.92 934 001	5.97 270 373	100.0	0.1 048 527 794 880 441 [−02]
			2.0	0.1 046 003 446 557 635 [−02]
			0.2	0.2 845 303 344 710 229 [−04]
	17.42 010 556	10.32 300 145	100.0	0.6 034 893 880 611 726 [−04]
			2.0	0.6 034 882 729 963 596 [−04]
			0.2	0.8 940 252 471 318 926 [−05]
(−1,6,4)	0.62 450 527	0.41 287 135	100.0	0.1 994 011 581 591 710 [+12]
			2.0	0.3 251 278 249 022 441 [+03]
			0.2	0.1 201 445 408 496 434 [−08]
	8.92 934 001	5.97 270 373	100.0	0.2 402 841 809 704 088 [−02]
			2.0	0.1 563 929 754 689 225 [−02]
			0.2	0.1 788 104 352 520 599 [−09]
	17.42 010 556	10.32 300 145	100.0	0.2 982 994 019 928 102 [−05]
			2.0	0.2 960 593 408 759 482 [−05]
			0.2	0.4 140 724 390 264 580 [−10]

R they rapidly approach the destabilization limit. Hence the variation produces a "*knee*" around some particular value of R. For higher excited states, this "*knee*" appears at a higher value of R. Enlarged views of the destabilization regions for $1sns$ ($^1S^e$) [$n=1$–3] and $1sn'p$ ($^1P^o$) [$n'=2$–4] states of the C^{4+} ion are given in Figs. 1(b) and 1(d), respectively. All other ions also show the same features. Similar behavior of energy values of He-like ions inside a spherical impenetrable box (referred to as the "Coulombic sphere" hereinafter) was reported in a recent publication [53] where the potential inside the box was purely Coulombic. The comparison between an IS and a Coulombic sphere having same radius is interesting as, within an ion sphere, there is a uniform plasma electron density while in the Coulombic sphere, there is no plasma. Hence differences between the "*pure*" (or *free*) atomic model and the Coulombic sphere are due to the cutoff, while differences between the Coulombic sphere and the IS model are due entirely to the plasma. Therefore, within the ion sphere, the energy value of the positively charged ion is modified, as compared to a "*pure*" ion, due to two factors:

(1) The environment envisaged by the IS potential which is governed by plasma electron density *and*

(2) The truncation of wave function at a finite distance that generates a pressure on the system.

TABLE V. Convergence of energy values ($-E$ a.u.) of the $1s^2(\,^1S^e)$ state of C^{4+} with respect to number of terms (N) in wave function within the ion-sphere radius R a.u.

		$-E$ for two-electron ions				
State	N	$R=20.0$	0.7	0.5	0.47	0.4692
$1s^2(\,^1S^e)$	13	31.80 607 622	14.87 985 637	3.40 916 161	0.10 351 773	0.00 534 000
	22	31.80 626 559	14.88 059 032	3.40 925 286	0.10 370 540	0.00 553 914
	34	31.80 629 082	14.88 061 939	3.40 926 383	0.10 371 810	0.00 555 223
	50	31.80 629 351	14.88 062 562	3.40 926 610	0.10 371 980	0.00 555 423
	70	31.80 629 412	14.88 062 707	3.40 926 664	0.10 372 017	0.00 555 462
	95	31.80 629 431	14.88 062 746	3.40 926 678	0.10 372 026	0.00 555 471
	125	31.80 629 439	14.88 062 759	3.40 926 682	0.10 372 029	0.00 555 474
	161	31.80 629 443	14.88 062 763	3.40 926 683	0.10 372 029	0.00 555 475

TABLE VI. Energy eigenvalues ($-E$ a.u.) of C^{4+} and C^{5+} within the ion sphere of radius R a.u. Densities (per cm^3) are determined from the radius by using Eq. (4). The uncertainty of the calculated energy values is of the order of 10^{-6} a.u.

Plasma density	$-E$ for two-electron ions							$-E$ for one-electron ions				
	R	$1s^2$	$1s2s$	$1s3s$	$1s2p$	$1s3p$	$1s4p$	R	E_{1s}	E_{2s}	E_{2p}	E_{3p}
	C^{4+}							C^{5+}				
8.05(20)	20.0	31.806 294	20.622 433	18.819 815	20.493 660	18.782 365	18.183 990	21.544	17.651 901	4.152 167	4.151 006	1.298 528
1.50(21)	16.256	31.668 147			20.355 753	18.645 771	18.051 134	17.511	17.571 741	4.072 241	4.070 983	1.216 051
6.44(21)	10.0	31.206 629	20.025 353	18.234 022	19.895 956	18.195 421	17.626 905	10.772	17.303 930	3.806 085	3.804 210	0.941 359
1.88(22)	7.0					17.710 079	17.127 014	7.540	17.005 859	3.512 120	3.508 790	0.638 130
5.15(22)	5.0	30.009 311	18.848 891	17.115 098	18.714 486	17.073 177	16.164 573	5.386	16.608 855	3.126 251	3.119 111	0.239 771
8.32(22)								4.591			2.885 861	0.001 097
1.01(23)	4.0						14.979 005	4.309	16.262 009	2.796 224	2.783 284	
2.39(23)	3.0	28.420 442	17.332 928	15.017 054	17.183 256	15.108 681	12.307 491	3.232	15.685 381	2.266 340	2.237 178	
4.12(23)	2.5			13.431 934		13.720 854	9.562 152	2.693	15.225 721	1.855 508	1.812 626	
6.05(23)	2.2						6.922 023	2.370	14.850 960	1.512 931	1.468 923	
8.05(23)	2.0		15.256 681	10.320 034	15.180 308	11.114 072	4.454 707	2.154	14.539 678	1.207 836	1.175 386	
1.10(24)	1.8			8.209 279			1.315 545	1.939	14.160 665	0.797 941	0.799 140	
1.31(24)	1.7			6.840 488		8.309 520	0.736 221	1.831	13.938 515	0.529 722	0.563 106	
1.57(24)	1.6	24.999 764				7.004 681		1.723	13.689 353	0.200 592	0.283 113	
1.58(24)	1.596						0.030 797	1.719	13.678 753	0.186 970	0.271 734	
1.85(24)								1.632			0.003 072	
1.91(24)	1.5		12.478 314	3.173 818	12.790 730			1.616	13.407 990			
2.35(24)	1.4			0.691 166		3.506 751		1.508	13.087 774			
2.38(24)	1.3937			0.516 288				1.501	13.066 138			
2.47(24)	1.3761			0.015 255				1.482	13.004 619			
2.93(24)	1.3		10.292 255			1.124 349		1.400	12.720 153			
3.20(24)	1.263					0.096 911		1.360	12.569 908			
3.73(24)	1.2		8.722 057		9.902 622			1.293	12.293 555			
6.44(24)	1.0	20.674 940	3.865 288		6.473 522			1.077	11.190 638			
7.52(24)	0.95		2.091 381					1.023	10.841 350			
8.55(24)	0.91		0.434 054					0.980	10.532 355			
8.79(24)	0.9017		0.059 416					0.971	10.464 484			
8.84(24)	0.9				3.864 058			0.969	10.450 413			
1.25(25)	0.8				0.209 360			0.862	9.499 773			
1.27(25)	0.797				0.077 557			0.858	9.466 811			
1.88(25)	0.7	14.880 628						0.754	8.198 121			
5.15(25)	0.5	3.409 267						0.539	2.956 871			
6.21(25)	0.47	0.103 720						0.5063	1.497 759			
6.23(25)	0.4695	0.042 434						0.5057	1.470 782			
6.24(25)	0.4692	0.005 555						0.5054	1.454 571			

TABLE VII. Energy eigenvalues ($-E$ a.u.) of Al^{11+} and Al^{12+} within the ion sphere of radius R a.u. Densities (per cm^3) are determined from the radius by using Eq. (4). The uncertainty of the calculated energy values is of the order of 10^{-6} a.u.

Plasma density	$-E$ for two-electron ions							$-E$ for one-electron ions				
	R	$1s^2$	$1s2s$	$1s3s$	$1s2p$	$1s3p$	$1s4p$	R	E_{1s}	E_{2s}	E_{2p}	E_{3p}
	Al^{11+}							Al^{12+}				
2.21(21)	20.0	159.382 029	101.075 286	90.920 760	100.751 849	90.826 863	87.343 470	20.589	83.625 742	20.250 901	20.250 869	8.508 494
1.77(22)	10.0	157.732 211	99.426 741	89.277 651	99.102 949	89.183 005	85.713 789	10.294	82.751 557	19.377 826	19.377 385	7.638 134
5.17(22)	7.0	156.318 323	98.015 642	87.878 476				7.206	82.002 366	18.631 067	18.629 929	6.898 570
1.00(23)	5.617	155.158 153			96.533 764	86.640 729	83.249 437	5.782	81.387 603	18.019 768	18.017 402	6.297 680
1.42(23)	5.0				95.811 753	85.932 485	82.582 105	5.147	81.003 693	17.638 853	17.635 633	5.926 068
5.00(23)	3.285	150.992 205			92.391 567	82.632 916	79.441 867	3.382	79.179 940	15.840 819	15.830 292	4.207 565
6.56(23)	3.0	150.039 702	91.786 850	81.867 981				3.088	78.675 129	15.347 266	15.332 246	3.746 670
1.00(24)	2.607	148.385 508			89.814 745	80.216 318		2.684	77.798 403	14.495 335	14.473 891	2.966 481
2.21(24)	2.0	144.557 994	86.435 075	76.751 134	86.060 502	76.632 056	70.991 150	2.058	75.769 505	12.554 606	12.501 889	1.209 389
3.31(24)								1.8			11.309 886	0.084 801
5.25(24)	1.5	139.093 636	81.216 562	70.476 891	80.776 714	70.672 695	59.958 894	1.544	72.871 972	9.877 422	9.760 672	
1.77(25)	1.0	128.240 365	70.674 599	51.222 379	70.269 488	53.774 530	27.642 101	1.029	67.112 431	4.647 358	4.445 998	
2.43(25)	0.9				66.602 776		13.910 306	0.926	65.206 039	2.699 333	2.596 821	
3.10(25)	0.83			34.498 851	63.390 834		1.358 983	0.854	63.604 555	0.880 652	0.952 002	
3.21(25)	0.82						0.585 110	0.844	63.354 014	0.578 268	0.692 836	
3.31(25)	0.812						0.088 777	0.836	63.149 234	0.327 244	0.479 227	
3.46(25)	0.8		61.584 852	30.304 265				0.823	62.834 616		0.011 954	
5.17(25)	0.7	114.496 531	54.024 877	11.937 344	55.190 310	21.877 996		0.721	59.806 678			
5.64(25)	0.68			7.201 566				0.700	59.097 854			
6.16(25)	0.66			2.007 102				0.6794	58.347 614			
6.18(25)	0.6594			1.843 590				0.6788	58.324 454			
6.37(25)	0.65283			0.022 248				0.672	58.067 871			
6.45(25)	0.65					11.929 838		0.669	57.955 830			
7.81(25)	0.61					2.170 876		0.628	56.265 059			
8.08(25)	0.603					0.262 866		0.621	55.946 962			
8.10(25)	0.6025					0.124 062		0.6202	55.923 954			
8.11(25)	0.6021					0.012 689		0.6198	55.905 567			
1.41(26)	0.5	96.523 118	22.189 554		30.281 348			0.515	50.268 732			
2.08(26)	0.44		2.370 513					0.453	45.729 585			
2.14(26)	0.436		0.724 569					0.449	45.379 873			
2.15(26)	0.4351		0.347 428					0.448	45.300 161			
2.16(26)	0.43434		0.026 971					0.447	45.232 635			
2.77(26)	0.4				3.174 966			0.412	41.877 044			
2.87(26)	0.395				1.274 781			0.407	41.331 971			
2.95(26)	0.3918				0.020 739			0.403	40.974 430			
6.56(26)	0.3	49.123 982						0.309	26.244 361			
1.28(27)	0.24	8.502 491						0.247	6.577 159			
1.419(27)	0.232	0.362 136						0.239	2.673 160			
1.424(27)	0.2317	0.038 819						0.238	2.518 185			

TABLE VIII. Energy eigenvalues ($-E$ a.u.) of Ar^{16+} and Ar^{17+} within the ion sphere of radius R a.u. Densities (per cm^3) are determined from radius by using Eq. (4). The uncertainty of the calculated energy values is of the order of 10^{-6} a.u.

Plasma density	$-E$ for two-electron ions							$-E$ for one-electron ions				
	R	$1s^2$	$1s2s$	$1s3s$	$1s2p$	$1s3p$	$1s4p$	R	E_{1s}	E_{2s}	E_{2p}	E_{3p}
	Ar^{16+}							Ar^{17+}				
3.22(21)	20.0	310.507 205	196.041 306	175.755 299	195.578 034	175.620 951	168.619 605	20.408	160.750 518	39.250 638	39.250 583	16.751 038
2.58(22)	10.0	308.107 341	193.642 370	173.360 319	193.178 832	173.225 396	166.234 270	10.204	159.501 078	38.002 041	38.001 721	15.505 423
2.06(23)	5.0	303.308 425	188.850 886	168.600 563	188.385 210	168.461 043	161.553 149	5.102	157.002 621	35.510 327	35.507 887	13.037 578
9.55(23)	3.0						155.654 881	3.061	153.672 785	32.208 489	32.196 858	9.835 118
2.11(24)	2.3						151.183 198	2.347	151.140 923	29.720 258		
2.96(24)	2.057	289.590 037			174.748 078	155.284 420	148.653 416	2.099	149.859 811	28.470 821	28.436 728	6.367 203
3.22(24)	2.0	288.926 557	174.593 816	154.885 258	174.092 315	154.670 904	147.924 331	2.041	149.514 344	28.135 153	28.099 008	6.066 598
7.64(24)	1.5			147.515 430		147.294 212	137.296 178	1.531	145.362 038	24.149 851	24.065 320	2.548 088
1.22(25)								1.309			21.374 828	0.027 313
1.49(25)	1.2			139.209 711			123.092 431	1.224	141.218 060	20.283 441	20.102 175	
2.58(25)	1.0	265.062 279	151.634 784	129.063 495	150.887 572	129.848 525	105.387 057	1.020	137.084 181	16.548 570	16.250 296	
5.03(25)	0.8			109.499 582			72.434 154	0.816	130.907 580	11.023 329	10.593 320	
7.51(25)	0.7	244.788 710	140.318 457	92.135 024	131.230 710	97.682 171	44.281 500	0.714	126.516 643	6.834 684	6.481 745	
9.39(25)	0.65						25.066 379	0.663	123.824 592	4.030 093	3.846 749	
1.13(26)	0.61						6.173 887	0.622	121.360 487	1.249 801	1.311 525	
1.18(26)	0.6014						1.639 257	0.614	120.788 926	0.571 762	0.762 695	
1.19(26)	0.6			64.536 211				0.612	120.694 413	0.458 366	0.622 378	
1.201(26)	0.5987						0.228 118	0.6109	120.606 199	0.352 195	0.544 660	
1.203(26)	0.59843						0.067 636	0.6106	120.587 871	0.330 097	0.523 396	
1.24(26)								0.604			0.048 119	
2.06(26)	0.5	218.150 195	99.801 076	17.342 729	102.188 104	37.003 115		0.510	112.615 414			
2.19(26)	0.49			10.878 182				0.500	111.632 327			
2.33(26)	0.48			3.985 508				0.4898	110.609 857			
2.344(26)	0.4791			3.342 920				0.4889	110.515 854			
2.345(26)	0.47902			3.285 614				0.4888	110.507 440			
2.41(26)	0.47455			0.035 558				0.4842	110.035 148			
2.83(26)	0.45					8.128 548		0.4592	107.280 138			
3.053(26)	0.4387					0.218 634		0.448	105.912 248			
3.059(26)	0.43843					0.022 169		0.447	105.878 796			
4.03(26)	0.4		63.058 578		72.434 796			0.408	100.662 918			
6.01(26)	0.35		30.887 328					0.357	92.198 308			
7.87(26)	0.32		3.274 140					0.326	85.821 161			
8.01(26)	0.318		1.126 899					0.3245	85.350 316			
8.04(26)	0.3176		0.692 178					0.3241	85.255 417			

TABLE VIII. (*Continued.*)

Plasma density	$-E$ for two-electron ions							$-E$ for one-electron ions			
	R	$1s^2$	$1s2s$	$1s3s$	$1s2p$	$1s3p$	$1s4p$	R	E_{1s}	E_{2s}	E_{2p}	E_{3p}
8.05(26)	0.31751		0.594 121					0.3240	85.233 983			
8.09(26)	0.31698		0.014 841					0.323	85.107 902			
9.55(26)	0.3	156.809 245						0.306	80.799 235			
1.08(27)	0.288				0.703 578			0.294	77.402 624			
1.09(27)	0.2874				0.09 253			0.293	77.224 113			
3.22(27)	0.2	64.368 049						0.204	34.699 257			
4.42(27)	0.18	25.307 474						0.184	15.611 535			
5.15(27)	0.171	2.741 398						0.1745	4.631 691			
5.24(27)	0.1701	0.269 467						0.1736	3.429 550			
5.25(27)	0.17001	0.019 935						0.1735	3.308 080			

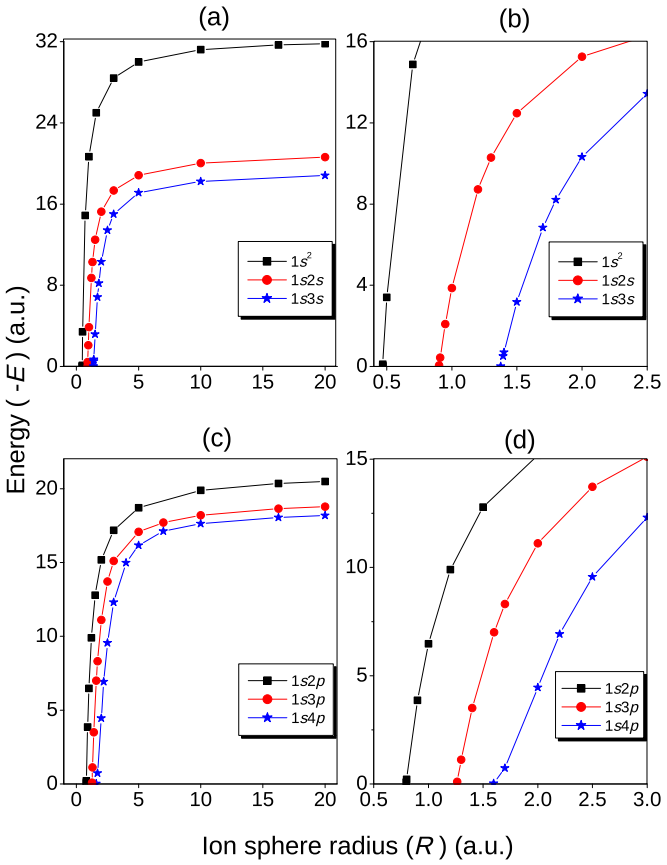

FIG. 1. (Color online) (a) Variation of eigenenergies ($-E$) of bound $1sns(^1S^e)$ [$n = 1$–3] states of C^{4+} with respect to the IS radius (R). (b) Enlarged view for $1sns(^1S^e)$ states near destabilization region. (c) Energies of $1sn'p(^1P^o)$ [$n' = 2$–4] states. (d) Enlarged view for $1sns(^1S^e)$ states near destabilization region.

In order to assess the effect of each factor on the energy eigenvalues, we have also studied separately the modification of energy values of two-electron ions due to the truncation of the wave function at different radii of the Coulombic sphere. The ground-state energy of a "*free*" C^{4+} ion where the wave function is infinitely extended is $-32.406\,247$ a.u. whereas within a Coulombic sphere and ion sphere both having a radius of 20.0 a.u, the energy values are $-32.406\,247$ and $-31.806\,294$ a.u., respectively. It shows that for a large box radius, almost 100% of the shift in the energy is due to the effect of plasma. The truncation of the wave function becomes significant when the size of the sphere is reduced. The effect of the truncation of the wave function on the total change in energy value can be calculated from $\frac{\Delta E_C}{\Delta E_{\rm IS}} \times 100\%$ where $\Delta E_C = E_C - E_f$, $\Delta E_{\rm IS} = E_{\rm IS} - E_f$, $E_f =$ energy of a "*free*" ion, $E_C =$ energy of the ion inside a Coulombic sphere, and $E_{\rm IS} =$ energy of the ion within an ion sphere of the same radius. At a radius of 0.7 a.u., the ground-state energy values of the C^{4+} ion within the Coulombic sphere and ion sphere are $-31.192\,275$ and $-14.880\,628$ a.u., respectively, which shows almost 7% of the total change of energy comes from the truncation of the wave function. This effect increases to 22.4% and 26.2% for the truncation radii of 0.5 and 0.4692 a.u., respectively.

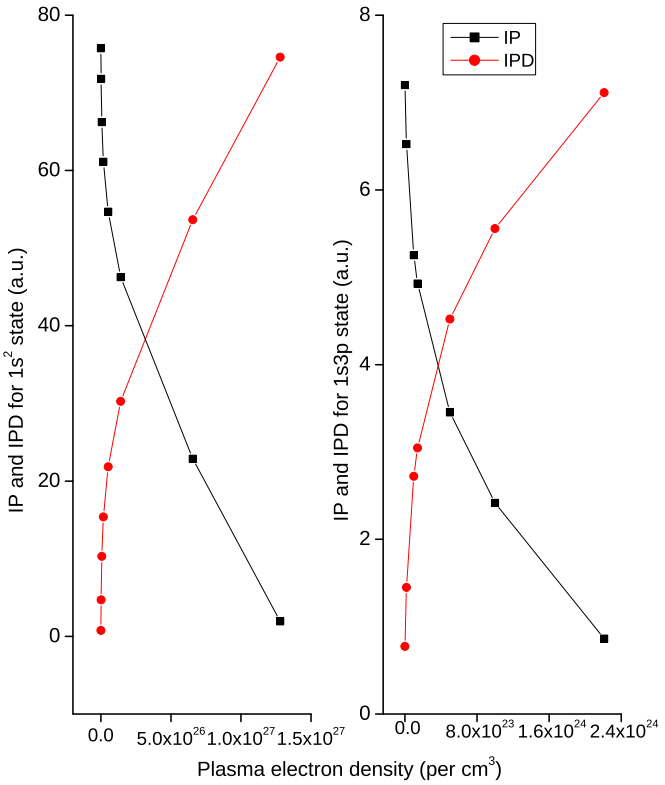

FIG. 2. (Color online) Variation of IP and IPD for $1s^2(^1S^e)$ and $1s3p(^1P^o)$ states of Al^{11+} with respect to plasma electron density.

A closer look at the results quoted in Tables VI–VIII leads us further to the following observations.

Decrease in number of excited states

For two-electron ions C^{4+}, Al^{11+}, and Ar^{16+} we see that as n_e increases, the ions become less bound and also the number of excited states decreases. For example, C^{4+} exists in the ground state up to $R = 0.4692$ a.u. but the $1s2s(^1S^e)$ state ceases to exist below $R = 0.9017$ a.u. and $1s3s(^1S^e)$ destabilizes below $R = 1.3761$ a.u. A similar feature is observed for all the ions and also for $^1P^o$ states. For H-like ions of C, Al, and Ar, the $2s$ state destabilizes much before $1s$ with decrease of R.

Reduction of ionization potential

Ionization potential for a two-electron ion is defined as the amount of energy required to ionize one electron from the ground state ($1s^2$). It is observed from Tables VI–VIII for all the ions that with increase in plasma density, IP decreases and beyond certain density, the two-electron energy levels move above the one-electron threshold. We have studied the variation of IPD of two-electron ions with respect to n_e from the difference of IP within and without (i.e., free case) the surrounding plasma environment. In Fig. 2, we have plotted the IP and IPD for Al^{11+} as a function of plasma electron density. The energy required to ionize the outer electron from the $1s3p(^1P^o)$ state, i.e., IP for the $1s3p(^1P^o)$ state of Al^{11+} and the corresponding IPD with respect to n_e are also included in Fig. 2. The effect of surrounding plasma on different two-electron energy levels should be different and consequently, IPDs should differ from one configuration to another. It is evident from Fig. 2 that the present observation corroborates this fact. The two-electron $^1P^o$ states would give rise to spectral lines via dipole transition until they merge into the one-electron continuum. For example, Table VII shows that the $1s3p(^1P^o)$ state of Al^{11+} can survive up to the density of $8.11 \times 10^{25}/cm^3$ whereas it crosses the corresponding $1s$ threshold after the density of $2.21 \times 10^{24}/cm^3$ and consequently, the He_β line originating from $1s3p(^1P^o) \rightarrow 1s^2(^1S^e)$ emission is not expected to be observed after this density. In Table IX, we have listed the critical electron densities after which different spectral lines of H-like and He-like Al disappear. The densities are calculated from the IS radius according to both the SP model and the EK model of determining IPDs following Eqs. (4) and (5), respectively. For the Ly_β line of Al^{12+} and the He_β line of Al^{11+}, the present electron densities calculated by using the SP model are in good agreement with experimental observation [43]. For disappearance of the He_γ line, the only theoretical calculation of plasma density is due to Preston *et al.* [41] where a possible range of densities is given. No experimental result is available for comparison in this context. Our results obtained by using the SP model of IPD indicate that the He_γ line of Al^{11+} would disappear after a plasma density of $5.0 \times 10^{23}/cm^3$, as is given in Table IX. We mention that the disappearance of both Ly_β and He_β lines are experimentally observed at the density of $2.21 \times 10^{24}/cm^3$ whereas the Ly_β line should survive more than the He_β line. Present results along with Ref. [47] as depicted in Table IX establish the fact explicitly. A more accurate experimental measurement is therefore necessary for proper plasma diagnostics.

In an earlier experiment, Nantel *et al.* [32] observed the He_α,He_β, and He_γ lines of C^{4+} at plasma density $1.5 \times 10^{21}/cm^3$. In this experiment the densities corresponding to the disappearance of such He-like lines are not explored. However, Table IX shows that the He-like lines of C^{4+} vanish well above the density of $1.5 \times 10^{21}/cm^3$. Hence, the existence of such He-like lines of C^{4+} at the density $1.5 \times 10^{21}/cm^3$ as observed by Nantel *et al.* [32] are consistent with present calculations. Similar comparisons have been done with other earlier experiments of Saemann *et al.* [33] and Woolsey *et al.* [34] for the spectral lines of Al^{11+} and Ar^{16+}, respectively, and the present results are in agreement with the experiments. Accurate measurement like the Orion laser experiment [43] is necessary to confirm the present theoretical predictions for the disappearance of the spectral lines of C^{4+} and Ar^{16+}.

Quasibound states of two-electron ions

Quasibound states or continuum bound states may be found in continuous parts of the spectra for electronic confinement under different potentials [61] and have also been observed experimentally [62]. These states have great structural similarity with the discrete energy levels. For a two-electron ion, the ground state and all singly excited energy levels, in general, lie below the first ionization threshold. Tables VI–VIII show that for high values "R" (i.e., almost free case), this feature is maintained for all the ions but as R decreases, all singly excited

TABLE IX. Critical plasma electron densities after which spectral lines of hydrogenlike and heliumlike Al disappear. Densities are obtained from IS radii according to both the SP model [Eq. (4)] and the EK model [Eq. (5)] for IPDs. The notation $x[y]$ indicates $x \times 10^y$.

		Critical plasma electron density (per cm^3)			
		Present results		Other results	
Z	Spectral line	SP model[a]	EK model[b]	Experiment	Theory
6	Ly_α	1.85[24]	1.19[24]		
	Ly_β	8.32[22]	2.77[22]		
	He_α	8.05[23]	1.61[23]		
	He_β	5.15[22]	1.03[22]		
	He_γ	1.88[22]	3.76[21]		
13	Ly_α	3.52[25]	2.71[24]		
	Ly_β	3.31[24]	2.55[23]	2.2[24][c]	2.93[24][d] 2.64[24]–3.3[24][e]
	He_α	2.43[25]	2.53[24]		
	He_β	2.21[24]	1.84[23]	2.2[24][c]	2.44[24][d] 1.98[24]–2.64[24][e]
	He_γ	5.00[23]	4.16[22]		6.60[22]–1.32[23][e]
18	Ly_α	1.24[26]	6.90[25]		
	Ly_β	1.22[25]	6.78[23]		
	He_α	7.51[25]	4.42[25]		
	He_β	7.64[24]	4.49[23]		
	He_γ	2.11[24]	1.25[23]		

[a]Reference [39].
[b]Reference [40].
[c]Reference [43].
[d]Reference [47].
[e]Reference [41].

states of two-electron ions become less bound more rapidly than the respective one-electron ion. For example, at $R = 20.0$ a.u. the energy values of C^{4+} as reported in Table VI lie below the $1s$ threshold of C^{5+}. At $R = 5.0$ a.u. the $1s4p(^1P^o)$ state moves above the $1s$ threshold but lies below the $2s$ threshold. Similarly, at $R = 2.0$ a.u. the $1s3s(^1S^e)$ and $1s3p(^1P^o)$ states lie above the $1s$ threshold and below the $2s$ threshold. At $R < 1.7$ a.u. the $2s$ level of C^{5+} destabilizes and we observe a well-converged (up to 7th significant digits) energy level of the $1s4p(^1P^o)$ state of C^{4+} embedded in one-electron continuum. A similar feature is obtained for other ions also and is being reported in SCP.

Incidental degeneracy and level crossing

For a free two-electron ion, the energy value of the $1s2s(^1S^e)$ state is more negative than the $1s2p(^1P^o)$ state. Tables VI–VIII establish this fact for high values of R corresponding to all the two-electron ions. For example, the $1s2s(^1S^e)$ level of C^{4+} lies below the $1s2p(^1P^o)$ level for the

TABLE X. Thermodynamic pressure on the ground state of one- and two-electron ions within the ion sphere. The conversion factor is as follows: 1 a.u. of pressure = 2.9421912(13) Pa. The notation $x[y]$ indicates $x \times 10^y$.

Plasma density	Pressure (Pa)		Plasma density	Pressure (Pa)		Plasma density	Pressure (Pa)	
	C^{4+}	C^{5+}		Al^{11+}	Al^{12+}		Ar^{16+}	Ar^{17+}
8.05(20)	0.1755[09]	0.8778[09]	2.21(21)	0.4829[09]	0.2414[10]	3.22(21)	0.7024[09]	0.3512[10]
6.44(21)	0.2807[10]	0.7019[10]	1.77(22)	0.7725[10]	0.1931[11]	2.58(22)	0.1123[11]	0.2809[11]
5.15(22)	0.4478[11]	0.5603[11]	5.17(22)	0.3217[11]	0.5630[11]	2.06(23)	0.1797[12]	0.2247[12]
2.39(23)	0.3432[12]	0.2581[12]	2.21(24)	0.4806[13]	0.2406[13]	3.22(24)	0.7007[13]	0.3504[13]
1.57(24)	0.4130[13]	0.1666[13]	1.77(25)	0.7580[14]	0.1899[14]	2.58(25)	0.1113[15]	0.2785[14]
6.44(24)	0.2779[14]	0.6681[13]	5.17(25)	0.3095[15]	0.5438[14]	2.06(26)	0.1729[16]	0.2818[15]
1.88(25)	0.1540[15]	0.1794[14]	1.41(26)	0.1178[16]	0.8791[14]	3.22(27)	0.9657[17]	0.3184[16]
5.15(25)	0.9278[15]	0.1772[14]	6.56(26)	0.1228[17]	0.1022[16]	4.42(27)	0.1667[18]	0.4212[16]
6.21(25)	0.1297[16]	0.9241[14]	1.28(27)	0.3912[17]	0.1489[16]	5.15(27)	0.2180[18]	0.8701[16]
6.23(25)	0.1304[16]	0.1123[15]	1.419(27)	0.4678[17]	0.2453[16]	5.24(27)	0.2241[18]	0.8897[16]
6.24(25)	0.1309[16]	0.1164[15]	1.424(27)	0.4710[17]	0.2466[16]	5.25(27)	0.2248[18]	0.8916[16]

IS radius down to $R = 2.0$ a.u. At $R = 1.5$ a.u., the $1s2s(^1S^e)$ state moves above the $1s2p(^1P^o)$ level. These results show that an "*incidental degeneracy*" [55] has taken place for the $1s2s(^1S^e)$ and $1s2p(^1P^o)$ states of C^{4+} at some value of R between 1.5 and 2.0. a.u. and then a "*level crossing*" occurs between two states having different symmetry properties. The phenomenon of *incidental degeneracy* was reported in the case of the shell-confined hydrogen atom by Sen [55] where two initially nondegenerate states are brought to the same energy level by adjusting external parameters. For a two-electron ion, we report *incidental degeneracy* within an SCP environment. After the *level crossing*, the $1s2s(^1S^e)$ state of C^{4+} destabilizes (at $R = 0.9017$ a.u.) much before the $1s2p(^1P^o)$ state (at $R = 0.797$ a.u.). Similarly, for the $1s3s(^1S^e)$ and $1s3p(^1P^o)$ states of C^{4+}, *incidental degeneracy* and subsequent *level crossing* are observed at a value of R lying somewhere between 5.0 and 3.0 a.u. We observe similar phenomena for other ions also. For the $2s$ and $2p$ states of H-like ions embedded in SCP, "*incidental degeneracy*" and "*level crossing*" phenomena are evident from Tables VI–VIII and are being reported here.

The thermodynamic pressure experienced by H-like and He-like C, Al, and Ar in their respective ground states have been calculated for different values of the IS radius R using Eq. (11) and the results are given in Table X. It is clear from Table X that as n_e increases, the pressure upon the ion increases and the ion moves towards destabilization. We observe that for a low value of n_e, the pressure upon the one-electron ion is higher than the respective two-electron ion and after a certain increase of n_e, the pressure on the two-electron ion exceeds the pressure experienced by the corresponding one-electron ion. With a view to studying the variation of thermodynamic pressure (P) with respect to the IS volume (V) under an adiabatic expansion, we have tried to fit the results for the two-electron ions obtained from the present calculations according to the ideal gas relation,

$$PV^{\gamma} = \text{constant} \quad \text{or} \quad \ln P + \gamma \ln V = \text{constant}, \tag{19}$$

where γ is the ratio of two specific heats. From a least square fit of the $\ln P$ vs $\ln V$ plot, the value of γ comes out to be close to 1.4 for all the two-electron ions. To be precise, for C^{4+}, Al^{11+}, and Ar^{16+}, the values of γ are 1.41, 1.37, and 1.37, respectively.

IV. CONCLUSION

Accurate analytical evaluation of the two-electron correlated integrals in Hyllerass coordinates within a finite limit has been performed. The intricacies of such calculations have been discussed in detail and the general applicability of these integrals has been established for arbitrary values of physically acceptable parameters. This methodology has potential to be useful for evaluation of the energy values and other spectral properties for three-body ionic and exotic systems placed within different external confinements such as strongly and moderately coupled plasma, fullerene cages, barrier potential, potential well, etc. With the recent advancement in experimental technique, the present methodology becomes relevant for calculating accurate plasma electron density from the spectral analysis of hydrogen and heliumlike ions. We conclude that, within an average atom approach, the ion-sphere potential where the electron density is calculated by using the SP model of IPDs provides a realistic picture of ions embedded in the SCP environment. The present nonrelativistic results reported here can be useful for plasma diagnostics and the nonrelativistic energy values can serve as a benchmark for future calculations to estimate relativistic and QED effects on two-electron ions within the finite domain.

ACKNOWLEDGMENTS

The authors are grateful to Dr. G. Dixit of Max Born Institute, Berlin, Germany for stimulating discussions on a recent experimental scenario. S.B. acknowledges financial support under Grant No. PSW-160/14-15(ERO) from University Grants Commission, Government of India. T.K.M. acknowledges financial support under Grant No. 37(3)/14/27/2014-BRNS from the Department of Atomic Energy, BRNS, Government of India.

[1] J. Sabin and E. Brandas (eds.) and prefaced by S. A. Cruz, Adv. Quantum Chem. **58** (2009).
[2] P. A. Jacobs, *Carboniogenic Activity of Zeolites* (Elsevier, Amsterdam, 1997).
[3] Y. B. Xu, M. Q. Tan, and U. Becker, Phys. Rev. Lett. **76**, 3538 (1996).
[4] A. N. Sil, S. Canuto, and P. K. Mukherjee, Adv. Quantum Chem. **58**, 115 (2009) and references therein.
[5] S. Canuto (ed.), *Solvation Effects on Molecules and Biomolecules, Computational Methods and Applications* (Springer, Berlin, 2008).
[6] C. A.Walsh, J. Yuan, and L. M. Brown, Philos. Mag. A **80**, 1507 (2000).
[7] M. Koskinen, M. Manninen, and S. M. Reimann, Phys. Rev. Lett. **79**, 1389 (1997).
[8] J. Cioslowski and E. D. Fleischmann, J. Chem. Phys. **94**, 3730 (1991).
[9] L. Turker, Int. J. Hydrogen Energy **32**, 1933 (2007).
[10] T. Guillot, Planet Space Sci. **47**, 1183 (1999).
[11] J. K. Saha, S. Bhattacharyya, and T. K. Mukherjee, Int. Rev. At. Mol. Phys. **3**, 1 (2012).
[12] J. K. Saha, S. Bhattacharyya, P. K. Mukherjee, and T. K. Mukherjee, J. Quant. Spec. Rad. Trans. **111**, 675 (2010).
[13] J. K. Saha, S. Bhattacharyya, P. K. Mukherjee, and T. K. Mukherjee, J. Phys. B **42**, 245701 (2009).
[14] A. F. Ordonez-Lasso, J. C. Cardona, and J. L. Sanz-Vicario, Phys. Rev. A **88**, 012702 (2013).
[15] L. G. Jiao and Y. K. Ho, Phys. Rev A **87**, 052508 (2013).
[16] M. Das, M. Das, R. K. Chaudhuri, and S. Chattopadhyay, Phys. Rev. A **85**, 042506 (2012).

[17] S. B. Zhang, J. G. Wang, and R. K. Janev, Phys. Rev. Lett. **104**, 023203 (2010).
[18] M. Das, R. K. Chaudhuri, S. Chattopadhyay, U. S. Mahapatra, and P. K. Mukherjee, J. Phys. B **44**, 165701 (2011).
[19] J. P. Santos, A. M. Costa, J. P. Marques, M. C. Martins, P. Indelicato, and F. Parente, Phys. Rev. A **82**, 062516 (2010).
[20] A. I. Akhiezer, I. A. Akhiezer, R. A. Polovin, A. G. Sitenko, and K. N. Stepanov, *Plasma Electrodynamics, Linear Response Theory*, Vol. 1 (Pergamon, Oxford, 1975).
[21] S. Ichimaru, Rev. Mod. Phys. **54**, 1017 (1982).
[22] J. C. Slater, Phys. Rev. **51**, 846 (1937).
[23] B. J. B. Crowley, Phys. Rev. A **41**, 2179 (1990).
[24] M. W. C. Dharma-Wardana and F. Perrot, Phys. Rev. A **45**, 5883 (1992).
[25] J. Stein, I. B. Goldberg, D. Shalitin, and D. Salzmann, Phys. Rev. A **39**, 2078 (1989).
[26] D. Salzmann, J. Stein, I. B. Goldberg, and R. H. Pratt, Phys. Rev. A **44**, 1270 (1991).
[27] C. A. Iglesias, Phys. Rev. A **29**, 1366 (1984).
[28] D. B. Boercker and C. A. Iglesias, Phys. Rev. A **30**, 2771 (1984).
[29] C. A. Iglesias, J. Quant. Spec. Rad. Trans. **54**, 181 (1995).
[30] J. Stein, J. Quant. Spec. Rad. Trans. **54**, 395 (1995).
[31] S. Alexiou, High Energy Density Physics **5**, 68 (2009).
[32] M. Nantel, G. Ma, S. Gu, C. Y. Cote, J. Itatani, and D. Umstadter, Phys. Rev. Lett. **80**, 4442 (1998).
[33] A. Saemann, K. Eidmann, I. E. Golovkin, R. C. Mancini, E. Andersson, E. Forster, and K. Witte, Phys. Rev. Lett. **82**, 4843 (1999).
[34] N. C. Woolsey, B. A. Hammel, C. J. Keane, C. A. Back, J. C. Moreno, J. K. Nash, A. Calisti, C. Mosse, R. Stamm, B. Talin, A. Asfaw, L. S. Klein, and R. W. Lee, Phys. Rev. E **57**, 4650 (1998).
[35] S. M. Vinko *et al.*, Nature Commun. **6**, 6397 (2015).
[36] S. M. Vinko *et al.*, Nature (London) **482**, 59 (2012).
[37] O. Ciricosta *et al.*, Phys. Rev. Lett. **109**, 065002 (2012).
[38] B. I. Cho *et al.*, Phys. Rev. Lett. **109**, 245003 (2012).
[39] J. C. Stewart Jr. and K. D. Pyatt, Astrophys. J. **144**, 1203 (1966).
[40] G. Ecker and W. Kröll, Phys. Fluids **6**, 62 (1963).
[41] T. R. Preston, S. M. Vinko, O. Ciricosta, H. K. Chung, R. W. Lee, and J. S. Wark, High Energy Density Physics **9**, 258 (2013).
[42] D. R. Inglis and E. Teller, Astrophys. J. **90**, 439 (1939).
[43] D. J. Hoarty *et al.*, Phys. Rev. Lett. **110**, 265003 (2013).
[44] D. J. Hoarty *et al.*, High Energy Density Physics **9**, 661 (2013).
[45] B. J. B. Crowley, High Energy Density Physics **13**, 84 (2014).
[46] S. M. Vinko, O. Ciricosta, and J. S. Wark, Nature Commun. **5**, 3533 (2014).
[47] S.-K. Son, R. Thiele, Z. Jurek, B. Ziaja, and R. Santra, Phys. Rev. X **4**, 031004 (2014).
[48] A. N. Sil, J. Anton, S. Fritzsche, P. K. Mukherjee, and B. Fricke, Eur. Phys. J. D **55**, 645 (2009) and references therein.
[49] N. Aquino, A. Flores-Riveros, and J. F. Rivas-Silva, Phys. Lett. A **307**, 326 (2003).
[50] A. Flores-Riveros and A. Rodriguez-Contreras, Phys. Lett. A **372**, 6175 (2008).
[51] C. Laughlin and S. I. Chu, J. Phys. A: Math. Theor. **42**, 265004 (2009).
[52] A. Flores-Riveros, N. Aquino, and H. E. Montgomery Jr., Phys. Lett. A **374**, 1246 (2010).
[53] S. Bhattacharyya, J. K. Saha, P. K. Mukherjee, and T. K. Mukherjee, Physica Scripta **87**, 065305 (2013).
[54] H. E. Montgomery Jr. and V. I. Pupyshev, Phys. Lett. A **377**, 2880 (2013).
[55] K. D. Sen, J. Chem. Phys. **122**, 194324 (2005).
[56] A. K. Bhatia and A. Temkin, Rev. Mod. Phys. **36**, 1050 (1964).
[57] T. K. Mukherjee and P. K. Mukherjee, Phys. Rev. A **50**, 850 (1994).
[58] J. K. Saha, S. Bhattacharyya, P. K. Mukherjee, and T. K. Mukherjee, Chem. Phys. Lett. **517**, 223 (2011).
[59] J. A. Nelder and R. Mead, Comput. J. **7**, 308 (1965).
[60] J. K. Saha and T. K. Mukherjee, Phys. Rev. A **80**, 022513 (2009).
[61] E. A. Carrillo-Delgado, I. Rodriguez-Vargas, and S. J. Vlaev, PIERS Online **5**, 137 (2009) and references therein.
[62] F. Capasso, C. Sirtori, J. Faist, D. L. Sivco, S. G. Chu, and A. Y. Cho, Nature (London) **358**, 565 (1992).